CMNE/CILAMCE 2007
Porto, 13 a 15 de Junho, 2007

APPLICATION OF THE LOG-CONFORMATION TENSOR APPROACH TO THREE DIMENSIONAL VISCOELASTIC FLOWS

Alexandre M. Afonso[1,*], Manuel A. Alves[1], Fernando T. Pinho[2,3] and Paulo J. Oliveira[4]

1: Departamento de Engenharia Química
CEFT - Centro de Estudos de Fenómenos de Transporte,
Faculdade de Engenharia da Universidade do Porto
Rua Dr. Roberto Frias, 4200-465 Porto, Portugal
e-mail: {aafonso,mmalves}@fe.up.pt, web: http://www.fe.up.pt

2: Universidade do Minho,
Largo do Paço, 4704-553 Braga,
e-mail: fpinho@dem.uminho.pt, web: http://www.uminho.pt

3: CEFT - Centro de Estudos de Fenómenos de Transporte,
Faculdade de Engenharia da Universidade do Porto
Rua Dr. Roberto Frias, 4200-465 Porto, Portugal
e-mail: fpinho@fe.up.pt, web: http://www.fe.up.pt

4: Departamento de Engenharia Electromecânica
MTP – Unidade Materiais Têxteis e Papeleiros
Universidade da Beira Interior
6201-001 Covilhã, Portugal
e-mail: pjpo@ubi.pt, web: http://www.ubi.pt

Key words: Square/Square contraction; Viscoelastic flows; Log-conformation tensor; Finite-volume method.

Summary. *A finite-volume method is applied to the numerical simulation of creeping flows of viscoelastic fluids through a 4:1 square-square three dimensional abrupt contraction. The calculation of the polymer stress contribution is carried out with the log-conformation methodology [1]. The log-conformation scheme allowed converged solutions at higher Deborah numbers for the Oldroyd-B fluid than the standard method when imposing steady flow conditions, but not for the UCM model. This does not mean that the log-conformation technique is less effective for the UCM fluid, but suggests that this flow is most probably time-dependent above a critical Deborah number. In any case, this work confirms the advantages of the log-conformation approach vis-a-vis the standard procedure.*

1 INTRODUCTION

A finite-volume method is applied to the numerical simulation of laminar viscoelastic flows through a 4:1 square/square three dimensional abrupt contraction. The upper-convected Maxwell (UCM) and Oldroyd-B fluids (Old-B) [2,3], were selected for this study to analyse the applicability of the matrix logarithm formalism for Maxwell-type models in a flow with geometric singularities. It is well known that geometries with sharp corners, like contraction flows, pose a great challenge to numerical methods, especially at high Deborah numbers (a measure of the elasticity of the flow).

The flow of viscoelastic fluids in a planar 4:1 sudden contraction was selected as benchmark problem during the Fifth International Workshop on Numerical Methods in Non-Newtonian Flows in 1987 [4]. Owens and Phillips [5], McKinley et al. [6] and Boger [7] present comprehensive literature reviews on experimental studies in this flow. A wealth of numerical research has also been done, especially for the axisymmetric geometry. Extensive reviews of numerical investigations on both axisymmetric and planar contraction flows can be found in Keunings [8], Baaijens [9], Walters and Webster [10], Owens and Phillips [5] and Oliveira and Pinho [11]. More recently, the flow of Newtonian and Boger fluids in 3D square-square contractions flows was investigated experimentally by Alves et al. [12]. In this work an extensive set of flow visualizations is presented for the middle plane of a 4:1 square–square sudden contraction using a streakline photography technique. The authors reported the appearance of a lip vortex at high Deborah numbers for the more concentrated Boger fluid (PAA300 solution) and related the onset of lip vortex with the increase of shear induced normal stresses due to the secondary flow in the cross section of the rectangular channel.

An interesting flow feature was presented in the numerical work of Alves et al. [13] for a three-dimensional 4:1 square-square contraction flow. The fluid was described by using a multimode PTT model (with 4 modes) with a Newtonian solvent contribution. The experimental results and the numerical simulations showed significant vortex growth in the horizontal plane and, surprisingly, an inversion in the direction of the fluid particles flow due to elastic effects. This inversion, where the fluid particles streak lines enter to the vortex at the horizontal (or vertical) planes of symmetry and leave at the diagonal planes, was also predicted by Sirakov et al. [14] in the 3D 4:1 square to circular cross-section contraction simulations. The latter authors applied a three-dimensional finite element method to analyze the viscoelastic flow of branched LDPE through 3D planar contractions using the eXtended Pom–Pom (XPP) model.

In this work we have implemented the methodology recently proposed by Fattal and Kupferman [1], the so called matrix-logarithm or log-conformation formulation (denomination used henceforth) for the viscoelastic constitutive equations, which is based on a reformulation of the constitutive law in terms of the matrix logarithm of the conformation tensor. According to Fattal and Kupferman [1], this formulation introduces a better polynomial interpolation of the logarithm of the variables that exhibit an exponential growth near stagnation points with the added advantage of preserving the positive definiteness of the conformation tensor [1,15-19].

Fattal and Kupferman [1] also reported a breakthrough in the high Weissenberg number

problem (HWNP; like the Deborah number, the Weissenberg number measures the flow elasticity) in their numerical simulations with the Finitely-Extensible Nonlinear Elastic (FENE) Chilcott–Rallison model in a two-dimensional lid-driven cavity flow. Fattal and Kupferman [15] extended the log-conformation approach to an Oldroyd-B fluid in the same geometry using a multigrid solver, providing the possibility to perform stable simulations at very large values of the Weissenberg number. They also included a stability condition and stated that it may be very restrictive when convection is weak, as in creeping flows, and in the presence of large deformation rates, as in the flow around sharp corners.

Hulsen et al. [16] were the first to implement the log-conformation methodology in a finite element method and tested it in the benchmark flow of Oldroyd-B and Giesekus fluids past a confined circular cylinder. They reported an apparent unbounded convergence limit for the Giesekus model, whereas for the Oldroyd-B fluid the solution became unsteady at high Deborah numbers while exhibiting a strong mesh dependency, particularly for the normal stresses on the wake of the cylinder.

Kwon [17] investigated numerically the planar 4:1 contraction flow with the Leonov constitutive equation and found more stable computations using the log-conformation method than with the conventional approach. Kwon also concluded that the log-conformation approach may only be effective for constitutive equations that are proven globally stable and therefore the stability constraint has to be taken into serious consideration. In a sequel, Yoon and Kwon [18] obtained solutions for Deborah numbers in excess of 100 using finer meshes. These authors also presented solutions for the 4:1:4 contraction/expansion flow and obtained converged solutions for Deborah numbers higher than 10. In both geometries, the convergence limits decreased with mesh refinement. Recently, Kwon [19] extended the log conformation formulation to viscoelastic flows around asymmetric arrays of cylindrical obstacles confined in a channel and the results agreed qualitatively with the flow characteristics.

Coronado et al. [20] presented a simple alternative implementation of the log-conformation formulation and simulated the planar Couette flow and the flow past a circular cylinder in a channel for several viscoelastic fluids modeled by generalized constitutive models. Their results demonstrated that the method works well for the generalized constitutive model improving the numerical stability at high *De*, especially in the flow past a confined cylinder, where the maximum *De* was extended to 1.0, as compared to 0.7 obtained with the standard DEVSS-TG/SUPG method. Their results were also in good agreement with those presented by Hulsen et al. [16].

In previous works we investigated the behaviour of the log-conformation formulation in the Finite Volume Method framework for creeping flows of viscoelastic fluids in steady and unsteady flow through a two dimensional 4:1 abrupt contraction [21,22]. The UCM and Oldroyd-B constitutive equations were used to assess the effect of different rheological behaviour on the flow patterns and solution stability. It was found that up to the critical conditions, when both methods converge to a steady solution, the use of the log-conformation technique provides solutions with similar accuracy as the standard approach. In terms of stability the log-conformation formulation is found to be more robust, and solutions could be

obtained at very high Deborah number flows, although in some cases elastic instabilities emerge.
The remainder of this paper is organised as follows: after presenting the governing equations, the log-conformation approach is described. Then, we introduce a set of parameters used to analyse the loss of evolution phenomenon. Prior to the presentation of results we briefly describe the numerical method used and present the geometry and computational meshes. The paper ends with the main conclusions.

2 GOVERNING EQUATIONS

To simulate steady incompressible creeping flows of viscoelastic fluids, the following set of governing equations needs to be solved: conservation of mass,

$$\nabla \cdot \mathbf{u} = 0 \tag{1}$$

conservation of linear momentum:

$$\rho \frac{D\mathbf{u}}{Dt} = -\nabla p + \beta \eta_o \nabla \cdot \left(\nabla \mathbf{u} + \nabla \mathbf{u}^T\right) + \frac{\eta_o}{\lambda}(1-\beta)\nabla \cdot \mathbf{A} \tag{2}$$

and a constitutive equation describing the evolution of the conformation tensor, **A**,

$$\mathbf{A} + \lambda \overset{\nabla}{\mathbf{A}} = \mathbf{I} \tag{3}$$

where $\overset{\nabla}{\mathbf{A}}$ represents Oldroyd's upper convected derivative, **I** the unit tensor, **u** the velocity vector, p the pressure and λ the relaxation time of the polymer. The viscosity ratio β is defined as the ratio between the Newtonian solvent viscosity, η_s, and the total zero shear rate viscosity, η_o,

$$\beta \equiv \frac{\eta_s}{\eta_o} = \frac{\eta_s}{\eta_s + \eta_P} \tag{4}$$

where η_P is the polymer viscosity coefficient, and it allows selection from the two quasi-linear constitutive models used in this work: if $\beta = 0$ then the system of equations (2-3) defines the upper-convected Maxwell (UCM) fluid and if $0 < \beta < 1$ the Oldroyd-B model [2,3]. For $\beta = 1$ equation (2) reduces to the standard Navier-Stokes equations valid for a Newtonian fluid. Here, $\beta = 0.59$ is used for the Oldroyd-B simulations. The constitutive law written in terms of the conformation tensor **A**, can be explicitly formulated as a function of the polymer contribution to the extra stress tensor, $\boldsymbol{\tau}$, with the following relation valid for both models,

$$\boldsymbol{\tau} = \frac{\eta_p}{\lambda}\left(\mathbf{A} - \mathbf{I}\right) \tag{5}$$

and thus, the system of the governing equations can be written explicitly in terms of the extra stress tensor. The formulation in terms of the extra stress tensor is frequently used, and was adopted in our previous works [11-13, 23-26].

2.1 The *log-conformation* representation

As mentioned above, Fattal and Kupferman [1] suggested a logarithmic transformation of the conformation tensor for differential viscoelastic constitutive equations. The core feature of the transformation is the decomposition of the velocity gradient, $\nabla\mathbf{u}$, into a traceless extensional component, **E**, and a pure rotational component, **R** (for details, see Ref. [1]). With this decomposition, the constitutive law (3), can be re-written as [1]

$$\frac{\partial \mathbf{A}}{\partial t} + (\mathbf{u}\bullet\nabla)\mathbf{A} - \left(\mathbf{RA} - \mathbf{AR}\right) - 2\mathbf{EA} = \frac{1}{\lambda}\left(\mathbf{I} - \mathbf{A}\right) \tag{6}$$

In the log-conformation approach equation (6) is replaced by an equivalent equation for the logarithm of the conformation tensor, $\boldsymbol{\Theta} = \log \mathbf{A}$, benefiting from the fact that **A** is a symmetric positive definite (SPD) matrix, and thus can always be diagonalized into the form

$$\mathbf{A} = \boldsymbol{\Omega}\mathbf{D}\boldsymbol{\Omega}^T = \boldsymbol{\Omega}^T\mathbf{D}\boldsymbol{\Omega} \tag{7}$$

where $\boldsymbol{\Omega}$ is an orthogonal matrix made with the eigenvectors of matrix **A** and **D** is a diagonal matrix made with the corresponding three distinct eigenvalues of matrix **A**. The transformation from equation (6) to an equivalent equation for $\boldsymbol{\Theta}$ is straightforward, and leads to [1]

$$\frac{\partial \boldsymbol{\Theta}}{\partial t} + (\mathbf{u}\bullet\nabla)\boldsymbol{\Theta} - \left(\mathbf{R}\boldsymbol{\Theta} - \boldsymbol{\Theta}\mathbf{R}\right) - 2\mathbf{E} = \frac{\mathrm{e}^{-\boldsymbol{\Theta}}}{\lambda}\left(\mathbf{I} - \mathrm{e}^{\boldsymbol{\Theta}}\right) = \frac{1}{\lambda}\left(\mathrm{e}^{-\boldsymbol{\Theta}} - \mathbf{I}\right) \tag{8}$$

2.2 Loss of evolution

The positive definiteness of the conformation tensor is known to be crucial for well posedness of the evolution equation [27,28]. Nevertheless, some degree of loss of evolution has been found in constitutive equations proven to be stable under short and high frequency wave disturbances (Hadamard stability, Dupret and Marchal [27] and Lee et al. [28]).
In this work, the criterion followed to assess the loss of evolution was to check the determinant of the conformation tensor during the iterative procedure; if $\det \mathbf{A} < 0$, then the positive definiteness of tensor **A** is violated.

3 NUMERICAL METHOD

Over the last decade, our group have been developing a finite-volume method (FVM) to calculate viscoelastic flows using various differential rheological constitutive equations for the polymer contribution to the extra stress tensor [11-13,23-26]. It is a fully-implicit FVM, based on a time marching pressure-correction algorithm and formulated with the collocated variable arrangement. A detailed description of the method can be found in Oliveira et al. [25] and Alves et al. [26]. In this work the methodology was extended to the log-conformation procedure and the corresponding modifications are explained below.

The governing equations are initially transformed to a non-orthogonal system, but keeping the Cartesian velocity and conformation/log-conformation tensor components. The log-conformation tensor evolution equation can thus be written into a general non-orthogonal coordinate system ($\varsigma_1, \varsigma_2, \varsigma_3$), using now index notation for clarity, as

$$\frac{\partial J\Theta_{ij}}{\partial t} + \frac{\partial}{\partial \varsigma_k}\left(u_k \beta_{lk} \Theta_{ij}\right) = J\left(R_{ik}\Theta_{kj} - \Theta_{ik}R_{kj}\right) + 2JE_{ij} + \frac{J}{\lambda}\left(\mathrm{e}^{-\Theta_{ij}} - \delta_{ij}\right) \tag{12}$$

where J is the Jacobian of the transformation $x_i = x_i(\varsigma_l)$ and β_{lk} are metric coefficients defined as the cofactor of $\partial x_k / \partial \varsigma_l$.

After integration over the control volumes forming the computational mesh, and in time over a time step (δt), the β_{lk} coefficients are replaced by area components (index k) of the surface whose normal vector points towards direction l, the Jacobian J is replaced by the cell volume V, and the derivatives $\partial / \partial \varsigma_l$ become differences between values along direction l.

Then after the discretization, the various terms are assembled, in the form

$$a_P^{\Theta}\Theta_{ij,P} - \sum_F a_F^{\Theta}\Theta_{ij,F} = S_{\Theta_{ij}} + \frac{\lambda_P V_P}{\delta t}\Theta_{ij,P}^0 \tag{13}$$

where $\Theta_{ij,P}^0$ refers to the ij component of the log-conformation tensor at the previous time level, a_P^{Θ} represents the central coefficient, a_F^{Θ} represents the coefficients of the neighbouring cells (with F spanning the near-neighbouring cells of cell P) and $S_{\Theta_{ij}}$ is the total source term.

The discretised momentum equations are solved sequentially after assembling all coefficients and source terms, to obtain the three Cartesian velocity components u, v and w. As generally the velocity components do not satisfy the continuity equation, a pressure-correction field, obtained from a Poisson pressure equation, is solved with a symmetric conjugate gradient method preconditioned with an incomplete LU decomposition.

The advective term in equation (8) was discretized with three distinct differencing schemes: the first-order accurate scheme UDS (upwind differencing scheme), the formally third-order accurate scheme QUICK (Quadratic Upstream Interpolation Scheme for Convective Kinematics) [30] and the CUBISTA high resolution scheme of Alves et al. [26], formally of

third-order accuracy in uniform meshes and especially designed for differential viscoelastic constitutive equations.

4 FLOW GEOMETRY AND COMPUTATIONAL MESH

The flow geometry and boundary conditions are illustrated in **Figure 1(a)**. The full domain is used in the simulations in order to capture possible elastic flow asymmetries or instabilities that may developed. The half-width of the downstream channel H_2 is taken as the characteristic length scale and the average velocity in that channel U_2 is the characteristic velocity. Stresses are normalised with $T_w = \eta U_2 / H_2$. An inlet length of $L_1 = 40\ H_2$ and an outlet length $L_2 = 100\ H_2$ are used, both sufficient for complete flow development upstream and downstream of the contraction. At the entrance a uniform velocity profile is imposed, while at the exit null streamwise gradients are imposed to velocity and stress/conformation components and to the pressure gradient.

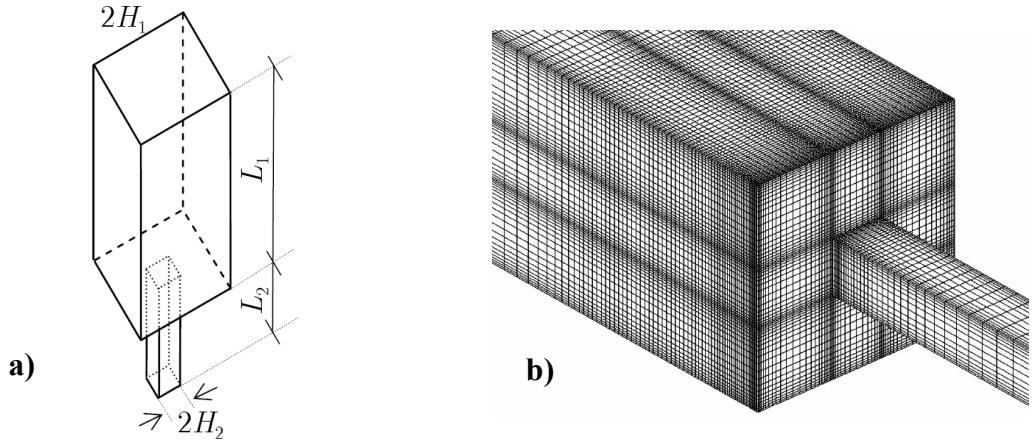

Figure 1: (a) Schematic representation of the Square/Square 4:1 contraction geometry and (b) detailed view near the contraction plane on mesh M56.

Calculations with the UCM and Oldroyd-B models, under creeping flow conditions, were carried out with two meshes, M40 and M56, whose major characteristics are listed in **Table 1**.

Table 1. Main characteristics of computational meshes.

	Number of cells	Degrees of freedom
M40	51 000	510 000
M56	312 816	3 128 160

The mesh data in **Table 1** includes the total number of control volumes in the meshes (NC) and the number of degrees of freedom (DOF). These computational meshes are orthogonal

but non-uniform, and the concentration of cells is higher near the corners of the contraction and the walls, where the stress/conformation tensor gradients are expected to be higher. A zoomed view of mesh M56 near the contraction plane is depicted in **Figure 1(b)**.
In order to assess the implementation of the log-conformation methodology described before, all simulations were carried out using two different formulations: the standard formulation using the extra stress tensor (i.e. without using the conformation tensor, see references [11-13,23-26]) and the formulation with the log-conformation tensor (for conciseness henceforth denoted ***strT*** and ***LogT***, respectively). In both formulations the L2-norm of the residuals of the equations was required to be less than a tolerance of 10^{-5}, in order to stop the time stepping procedure, and all the calculations were obtained with the same time step increment (δt). Increments in the relaxation time of the fluid, λ, at a fixed average velocity, allows a direct increase of the Deborah number, here defined based in the downstream conditions,

$$De = \frac{U_2 \lambda}{H_2} \tag{17}$$

In the next sections we present qualitative (flow patterns and 3D streaklines) and quantitative results (vortex sizes in diagonal and horizontal/vertical vortices, distribution of the first normal stress difference along the downstream channel wall and stability criteria). In section 5.1 we present results for the UCM model and in section 5.2 the results for the Oldroyd-B fluid.

5. RESULTS

5.1 UCM model

We start by presenting in **Figure 2** the theoretical and numerical profiles of streamwise velocity in the mid planes of the inlet and outlet square channels for fully developed flow. The numerical profiles are for both ***strT*** and ***LogT*** formulations at a Deborah number of 1.35 and along the lateral and out-of-depth directions. As we can see, the theoretical and numerical profiles collapse at this Deborah number, indicating that the inlet and outlet lengths (L_1 and L_2, respectively) used in the computational meshes, are sufficient for complete flow development upstream and flow redevelopment downstream of the contraction.
Results of the normalized vortex size in diagonal (X_{DR}) and horizontal/vertical (X_{HR}) planes for both the ***strT*** and ***LogT*** formulations, obtained on meshes M40 and M56 with three different interpolating schemes for the convective terms in the constitutive equation (UDS, QUICK and CUBISTA) are presented in **Figure 3**. We note that the vortex sizes are normalized with H_1 (and not with H_2 as for other variables): $X_{HR} = x_{HR}/H_1$; $X_{DR} = x_{DR}/H_1$.
In the three dimensional flows both the diagonal, X_{DR} (see **Figure 3a**), and horizontal/vertical, X_{HR} (see **Figure 3b**), vortex lengths increase significantly with Deborah number, in contrast with the two-dimensional abrupt contraction [11,21,22,24]. For Newtonian fluids good iterative convergence behaviour was obtained, independent of mesh refinement and

formulation and the X_{HR} values asymptotes to 0.326, in agreement with predictions by Alves et al. [12,13]. The X_{DR} values asymptotes to 0.554. When CUBISTA scheme is used in the finest mesh, steady-state solutions were obtained up to $De \approx 1.4$ for both the ***strT*** and ***LogT*** formulations. For the less refined mesh M40 and with the UDS scheme, steady simulations were obtained up to $De \approx 2.13$ for both the ***LogT*** and ***strT*** formulations.

It is well known that the UDS scheme introduces some numerical diffusion [11,23-24], as observed in the ***strT*** results (**Figures 3a and b**), where both horizontal and diagonal vortices are seem to deviate from the values obtained in a finest mesh with CUBISTA scheme. However, the UDS results obtained with the ***LogT*** formulation are closer to the results obtained with both a precise interpolation scheme and a finer mesh, showing that this formulation is not so sensitive with respect to the interpolation scheme. This result is not totally unexpected since a near exponential growth in the extra stress (or in the conformation) tensor results in a linear growth in the ***LogT*** formulation, which is less sensitive to the numerical precision of the interpolation scheme.

A linear relation exists between the diagonal and horizontal/vertical vortices lengths, as can be observed in **Figure 4**, where we plot X_{DR} *vs*. X_{HR} containing data from all formulations, mesh refinement and interpolation schemes.

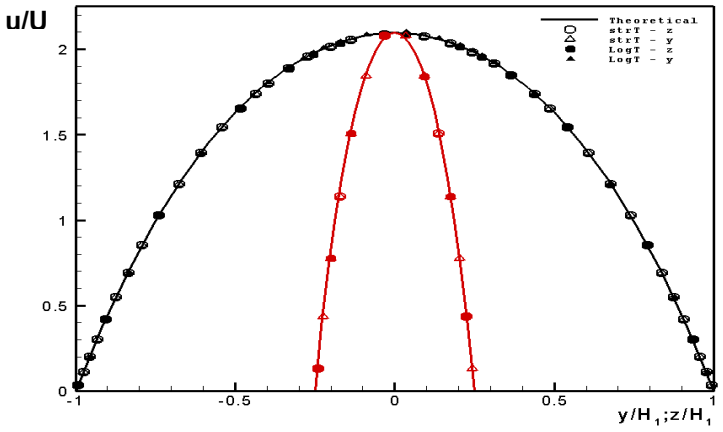

Figure 2: Theoretical and numerical axial velocity profiles along the lateral and out-of-depth directions at De=1.35 (mesh M56).

Figure 5 shows patterns of pathlines on the center plane of the geometry (y=0 or z=0) for both formulations (in the top and bottom half of each image) as function of Deborah number obtained on mesh M56.

Flow patterns are quite similar for both formulations over the whole range of Deborah numbers. **Figure 5** also includes the minimum values of the stability criterion, the value of $\det(\mathbf{A})_{min}$, which is approximately equal to one for all simulations. We may then assume that in these simulations numerical convergence and stability were attained.

Although at first look the recirculation flow seems to be closed, in reality the flow nature is three-dimensional and the recirculations are open. The three dimensional open recirculation in

a square-square abrupt contraction for the Newtonian fluid was already predicted by Alves et al. [12,13] and a description was presented and sketched in their figure 7. We recall the flow pattern for Newtonian flow in order to compare with the corresponding viscoelastic flow patterns. The streak lines of fluid particles departing from the top corner of the diagonal plane (points **A** and **A'** in **Figure 6**) enter the diagonal recirculation spiralling towards its center, then move along the eye of the recirculation to the vortex on the horizontal/vertical planes (**B** and **C** points) where it unwinds towards the walls and exits the contraction near the re-entrant corner.

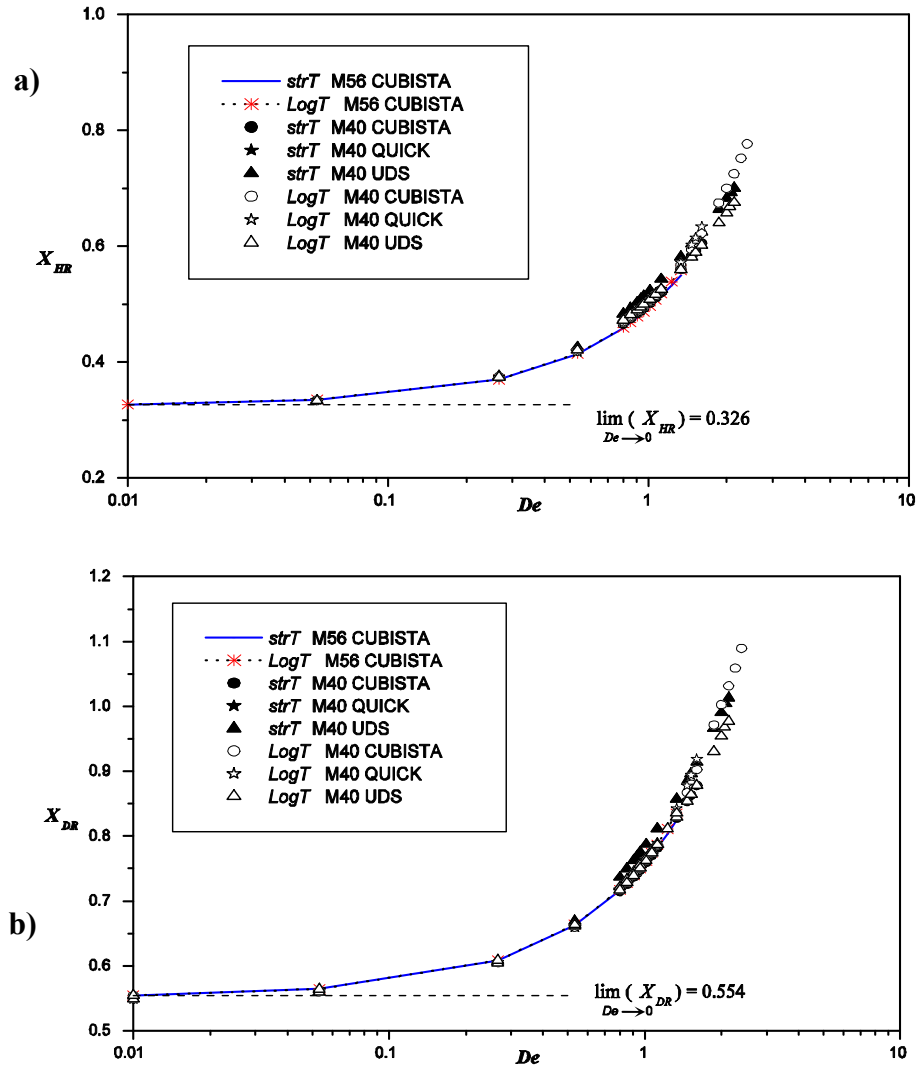

Figure 3: Dimensionless length of the (a) horizontal/vertical (X_{HR}) and (b) diagonal (X_{DR}) recirculation as a function of Deborah number obtained with meshes M40 and M56.

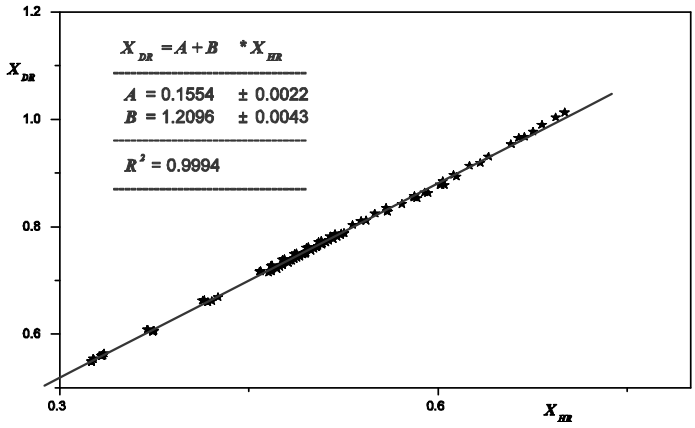

Figure 4: Linear relation between the diagonal and horizontal/vertical vortices lengths for UCM model.

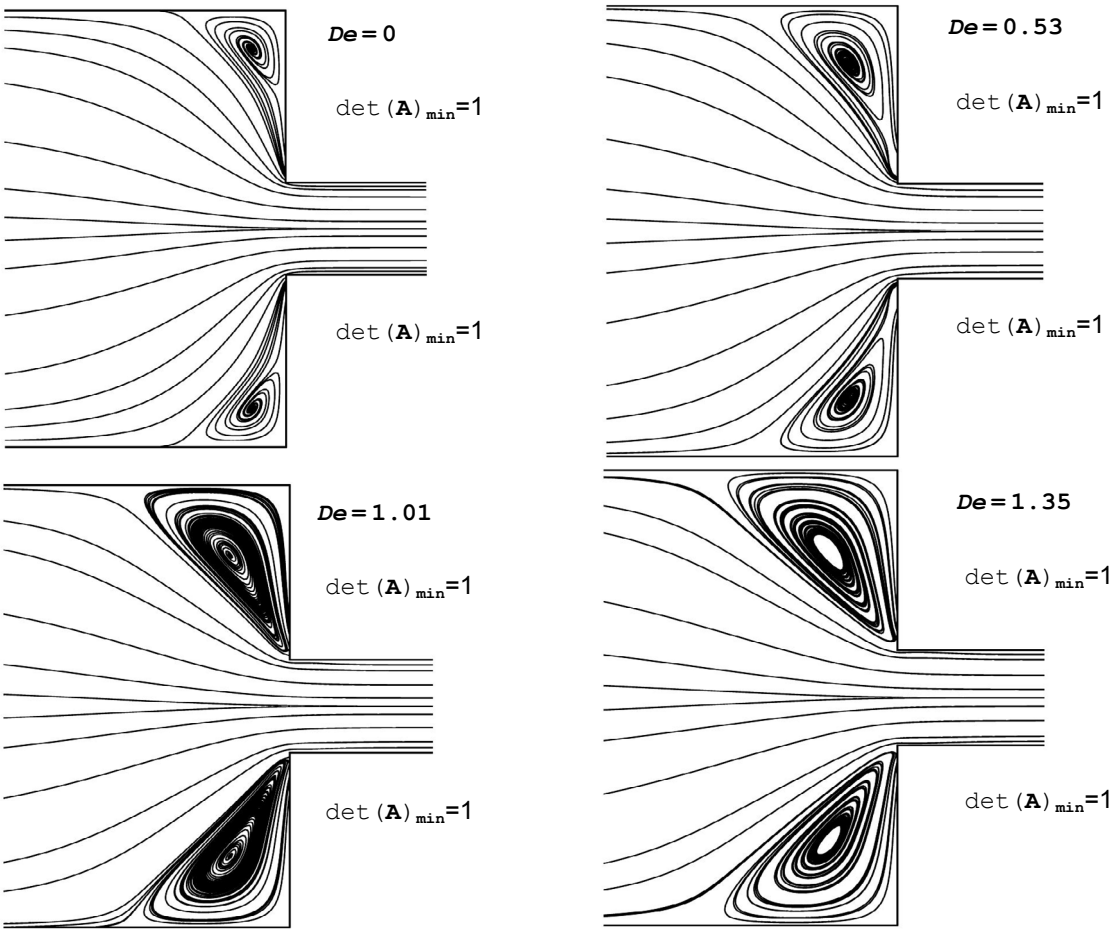

Figure 5: Flow patterns on the center plane predicted with mesh M56. (top half) ***strT***; (bottom half) ***LogT*** (except for *De*=0, where only ***strT*** prediction is shown) [$\det(A)_{min}$ – beside each map].

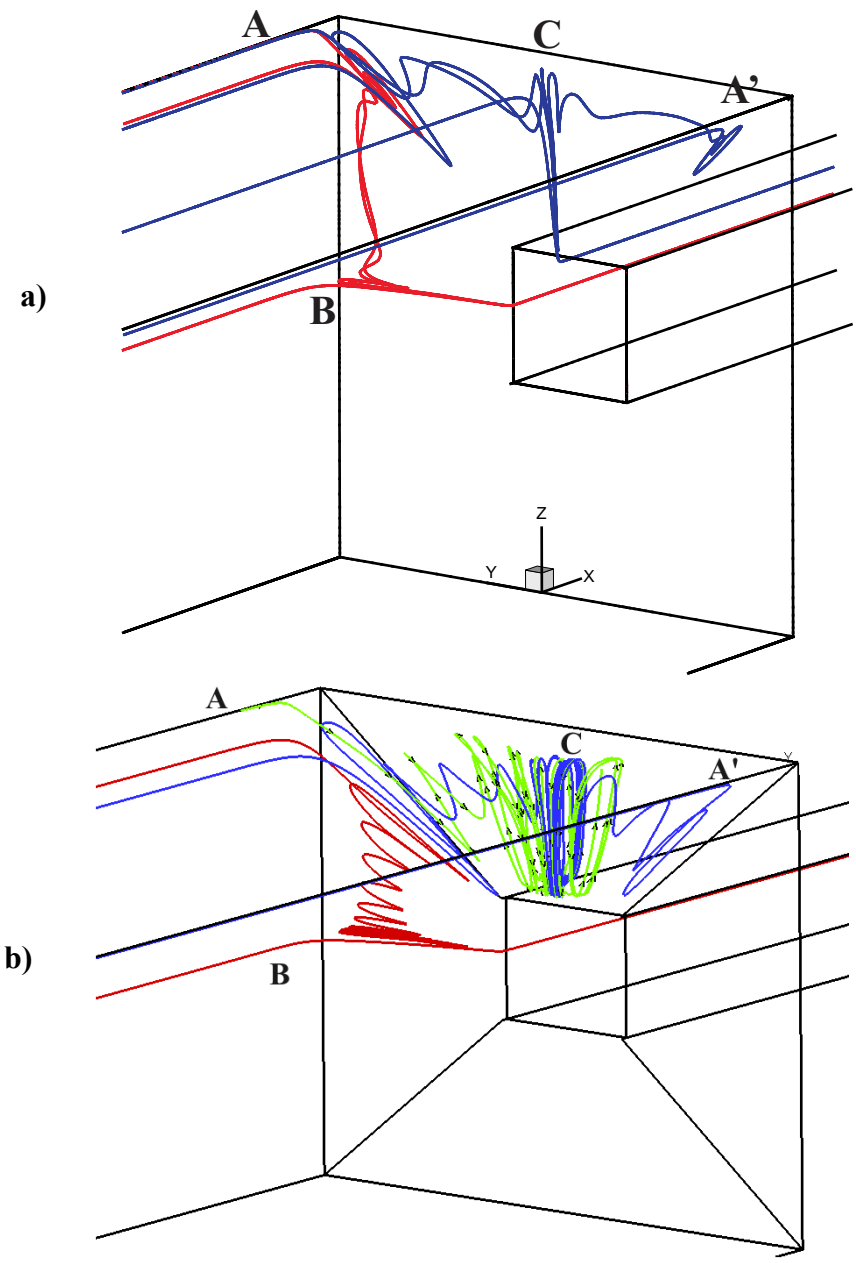

Figure 6: 3D particle trajectories: (a) Newtonian (***strT*** formulation); (b) *De*=1.35 (***LogT*** formulation).

In the viscoelastic simulation, with the UCM model at *De* = 1.35, the flow behaviour of the three dimensional flow in the recirculation is somewhat different and a much more complex flow is now observed, as sketched in **Figure 6b**. The vortices are now more intense than in the Newtonian case, and the spiralling motion is much more accentuated.

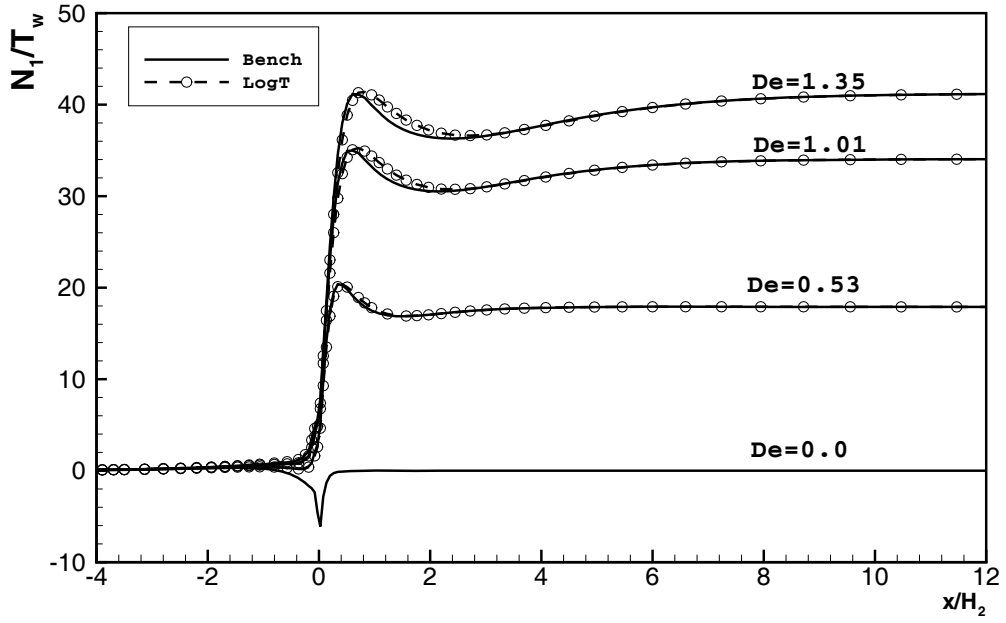

Figure 7: Distribution of the normalized first normal stress difference along the stream wise line that passes near the downstream channel wall (mesh M56 with CUBISTA scheme).

Finally, **Figure 7** presents the distribution of the normalized first normal stress difference along the line that passes near the downstream channel wall, calculated on mesh M56 with the CUBISTA scheme, for the ***strT*** and ***LogT*** formulations. For both formulations the N_1/T_w profiles in the stream wise direction increase with the Deborah number. The differences in the N_1/T_w profiles in the axial direction, near the downstream duct wall at $De \approx 1.35$ in the ***LogT*** formulation simulations, correlate with the onset of unsteady flow, as observed in the two-dimensional work by Afonso et al. [21,22].

5.2 Oldroyd-B model

In this section we analyse the effect of addition of a Newtonian solvent viscosity to the polymer, i.e. results are presented to an Oldroyd-B model having a viscosity ratio of $\beta = 0.59$.

As stated in the Introduction, the log-conformation approach may only work efficiently for constitutive equations that are proven globally stable, hence the stability constraint has to be taken into serious consideration [17]. This statement is confirmed if we compare the results obtained with the UCM and the Oldroyd-B models. With the former model, the critical Deborah numbers were small (up to $De \approx 1.4$ in the finest mesh) and the ***LogT*** formulation did not exceed the limit of the ***strT*** formulation results, at least in the steady state simulations. With the Oldroyd-B model, the onset of unsteady flow began at higher Deborah numbers and the critical *De* value obtained with the ***LogT*** formulation clearly exceeded those obtained with

the ***strT*** formulation (especially with mesh M40 and UDS scheme).
Figure 8 presents the results obtained for the normalized length of the diagonal (X_{DR}) and horizontal/vertical (X_{HR}) vortex for both the ***strT*** and ***LogT*** formulations, on meshes M40 and M56 with two different interpolating schemes (UDS and CUBISTA). Simulations with the QUICK scheme were also carried out, but are not presented here for conciseness. For the Oldroyd-B model, steady simulations were obtained up to $De\approx4.8$ and $De\approx5.1$ for the ***strT*** and ***LogT*** formulations, respectively, when the finest mesh is used with CUBISTA scheme, and the normalized vortex lengths of both the diagonal, X_{DR}, and horizontal/vertical, X_{HR} planes, increase significantly with Deborah number.

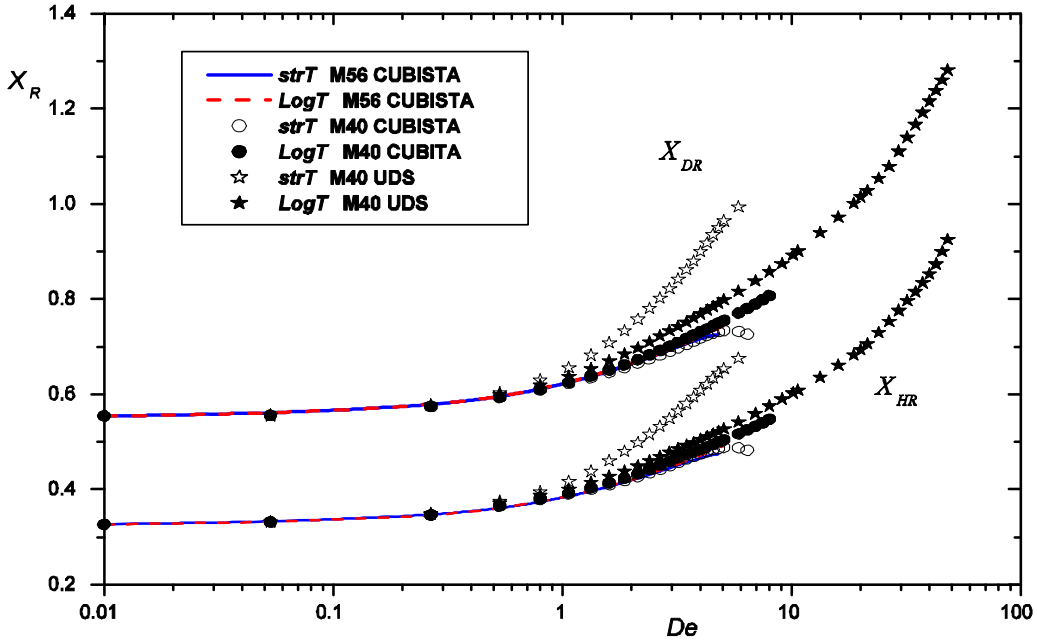

Figure 8: Dimensionless length of the diagonal (X_{DR}) and horizontal/vertical (X_{HR}) vortex as a function of Deborah number obtained with meshes M40 and M56 – Oldroyd-B fluid.

In the coarse mesh M40 with the CUBISTA scheme, the critical Deborah was $De\approx6.4$ and $De\approx8.0$ for the ***strT*** and ***LogT*** formulations, respectively, but with the ***LogT*** formulation and with UDS scheme the limit was obtained at higher Deborah numbers, $De\approx50$. As for the UCM results, the numerical diffusion introduced by the UDS scheme, was more intense in the ***strT*** results (**Figures 8**), where both the horizontal and diagonal vortex lengths deviate significantly from those obtained in the finest mesh with CUBISTA scheme. The maps of the streamline patterns on the center plane, obtained on mesh M56, are shown in **Figure 9** for both formulations (in the top and bottom half of each image) as a function of Deborah number. The streamlines patterns are quite similar for all Deborah numbers. The minimum value of the stability criterion for all simulations is approximately equal to one, meaning that

there is no loss of evolution and therefore stability was maintained in these simulations.

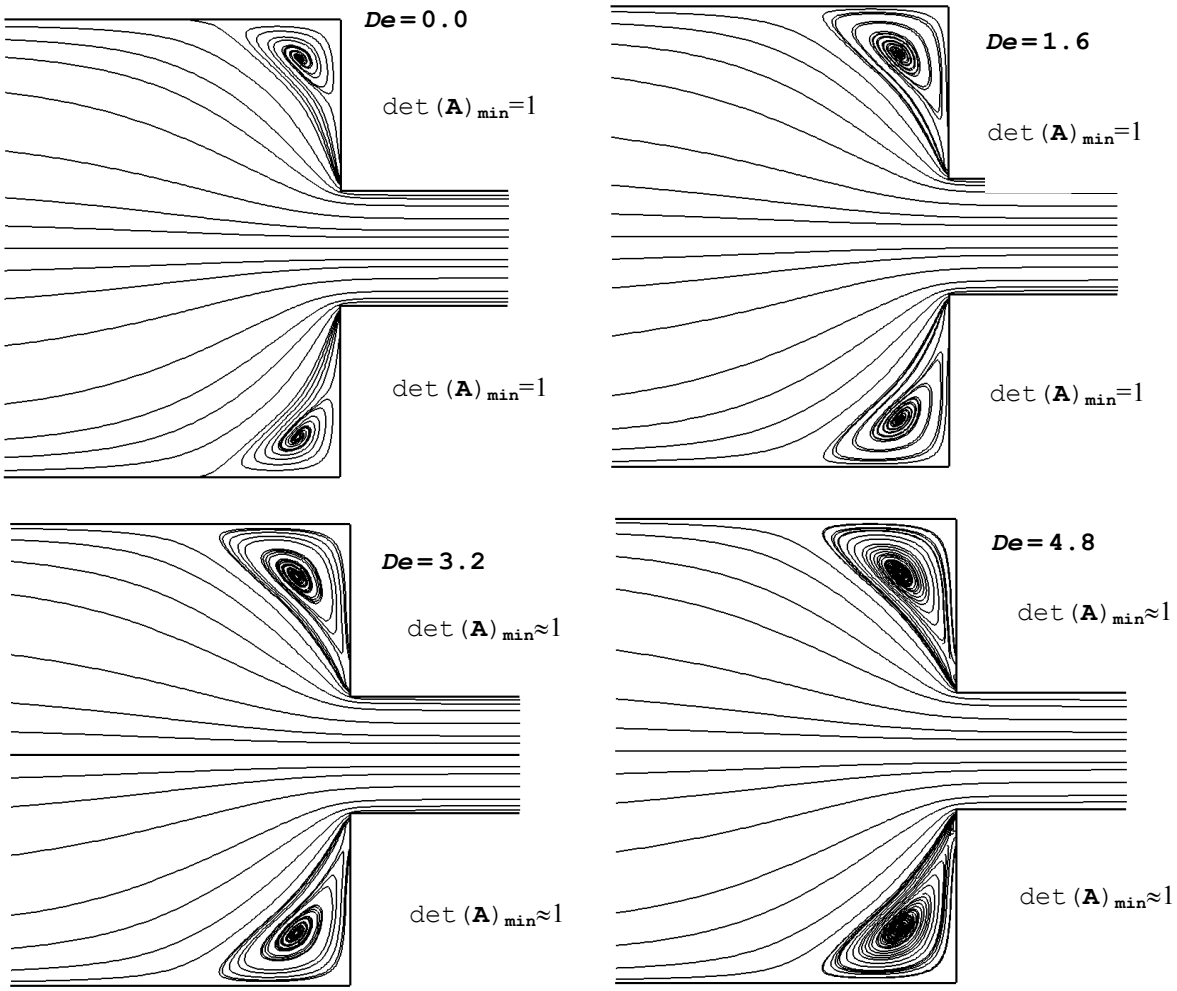

Figure 9: Flow patterns on the center plane predicted with mesh M56. (top half) ***strT***; (bottom half) ***LogT*** (except for *De*=0, where only ***strT*** prediction is shown) [det(A)$_{min}$ – beside each map] Oldroyd-B model.

The normalized first normal stress difference along the centreline that passes near the downstream channel wall, calculated on mesh M56 with the CUBISTA scheme, is shown in **Figure 10**, for the ***strT*** and ***LogT*** formulation. As in the UCM case, the N_1/T_w profiles in the axial direction increase with the Deborah number. Here again, the differences in the N_1/T_w in the axial direction, near the downstream duct wall near the critical Deborah number in the ***LogT*** formulation simulations can be correlated to the onset of unsteady flow.

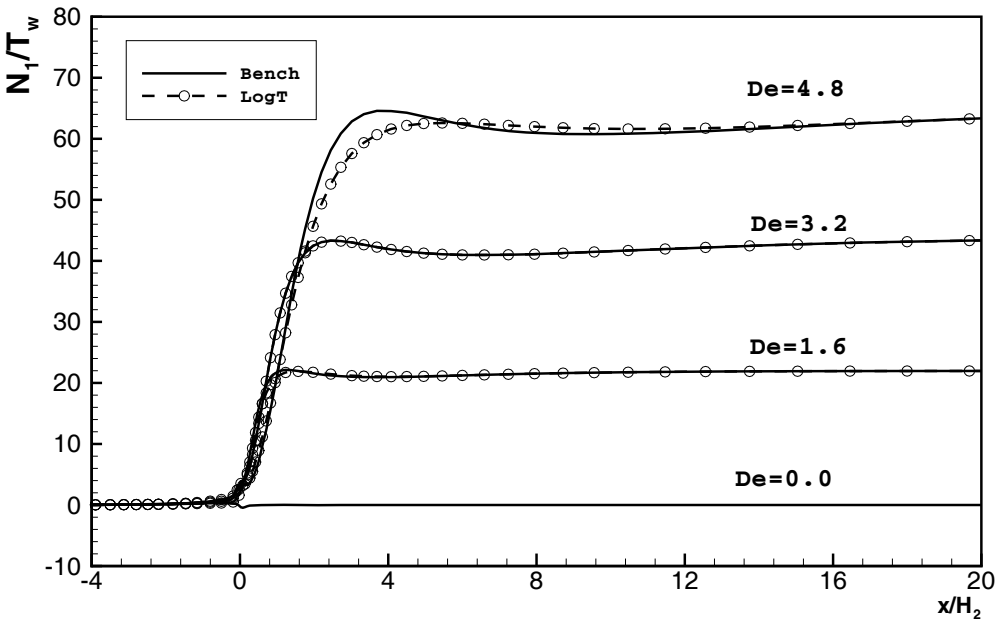

Figure 10: Distribution of the normalized first normal stress difference along the centreline that passes near the downstream conduct wall, calculated on mesh M56 with the CUBISTA scheme – Oldroyd-B fluid.

6 CONCLUSIONS

A new stress formulation was implemented into a finite-volume methodology and applied to the numerical simulation of three dimensional laminar viscoelastic flows through a square/square 4:1 abrupt contraction with the upper-convected Maxwell and Oldroyd-B fluids. This new logarithmic stress formulation (***LogT***) was contrasted against the usual stress formulation (***strT***) of previous works.

In the results obtained with the UCM model, the critical Deborah numbers were small (up to $De \approx 1.4$ on mesh M56) and similar for both the ***LogT*** and the ***strT*** formulations. However, with the Oldroyd-B model the onset of unsteady flow began at higher Deborah numbers (up to $De \approx 6.4$ on mesh M56) and the range of De for which steady results could be obtained with the ***LogT*** formulation clearly exceeded those obtained with the ***strT*** formulation (especially with mesh M40 and UDS scheme, with convergent and stable solutions up to $De \approx 50$). This does not mean that the log conformation formulation is less effective with the UCM fluid, it simply suggests that flows of these fluids are most probably time-dependent above the critical Deborah number.

It was also found that the new logarithmic formulation demonstrates to be much less sensitive to the use of the upwind scheme, yielding results that do not show the usual detrimental effect of numerical diffusion. This is an important result since upwind is the most robust differencing scheme to deal with the advective terms in the governing equations.

7 ACKNOWLEDGEMENTS

The authors acknowledge funding from FEDER and FCT through projects POCI/EQU/59256/2004, POCI/EQU/56342/2004 and POCI/EME/59338/2004. A. Afonso would also like to thank FCT for financial support through the scholarship SFRH/BD28828/ 2006.

REFERENCES

[1] R. Fattal and R. Kupferman, "Constitutive laws of the matrix-logarithm of the conformation tensor", *J. Non-Newt. Fluid Mech.* Vol. **123**, pp. 281-285, (2004).

[2] J.G. Oldroyd, "On the formulation of rheological equations of state", *Proc. R. Soc. Lond.* Vol. **A200**, pp. 523–541, (1950).

[3] R.B. Bird, R.C. Armstrong and O. Hassager, *Dynamics of polymeric liquids. Vol 1. Fluid mechanics*, 2nd Ed. Wiley, New York, (1987).

[4] O. Hassager, "Working Group on Numerical Techniques, in: Proceedings of the Vth Workshop on Numerical Methods in Non-Newtonian Flow", *J. Non-Newt. Fluid Mech.* Vol. **29**, pp. 2–5, (1988).

[5] R.G. Owens and T.N. Phillips, *Computational Rheology*, Imperial College Press, London, (2002).

[6] G.H. McKinley, W.P. Raiford, R.A. Brown and R.C. Armstrong, "Nonlinear Dynamics of Viscoelastic Flow in Axisymmetric Abrupt Contractions", *J. Fluid Mech*. Vol. **223**, pp. 411-456, (1991).

[7] D.V. Boger, "Viscoelastic flows through contractions", *Ann. Rev. Fluid Mech*. Vol. **19**, pp. 157–182, (1987).

[8] R. Keunings, *Simulation of viscoelastic flow*, in: C.L. Tucker (Ed.), Computer Modeling for Polymer Processing, Hanser, Munich, pp. 404–469, (1989).

[9] F.T.P. Baaijens, "Mixed finite element methods for viscoelastic flow analysis: a review", *J. Non-Newt. Fluid Mech*. Vol. **79** pp. 361–385, (1998).

[10] K. Walters and M.F. Webster, "The distinctive CFD challenges of computational rheology", *Int. J. Num. Meth. Fluids*, Vol. **45**, pp. 577–596, (2003).

[11] P.J. Oliveira and F.T. Pinho, "Plane contraction flows of Upper Convected Maxwell and Phan-Thien–Tanner fluids as predicted by a finite-volume method", *J. Non-Newt. Fluid Mech*. Vol. **88**, pp. 63-88, (1999).

[12] M.A. Alves, F.T. Pinho and P.J. Oliveira, "Visualizations of Boger Fluid Flows in a 4:1 Square–Square Contraction", *AIChE J.*, Vol. **51**, pp. 2908-2922, (2005).

[13] M.A. Alves, F.T Pinho and P.J. Oliveira, "Simulações numéricas de escoamento viscoelástico numa contracção tridimensional quadrada", *Métodos Computacionais em Engenharia*, Lisboa, (2004).

[14] I. Sirakov, A. Ainser, M. Haouche and J. Guillet, "Three-dimensional numerical simulation of viscoelastic contraction flows using the Pom–Pom differential constitutive model", *J. Non-Newt. Fluid Mech*. Vol. **126**, pp. 163–173, (2005).

[15] R. Fattal and R. Kupferman, "Time-dependent simulation of viscoelastic flows at high Weissenberg number using the log-conformation representation". *J. Non-Newt. Fluid Mech*., Vol. **126**, pp. 23–37, (2005).

[16] M. A. Hulsen, R. Fattal and R. Kupferman, "Flow of viscoelastic fluids past a cylinder at high Weissenberg number: Stabilized simulations using matrix logarithms", *J. Non-Newt. Fluid Mech*. Vol. **127**, pp. 27-39, (2005).

[17] Y. Kwon, "Finite element analysis of planar 4:1 contraction flow with the tensor-logarithmic formulation of differential constitutive equations", *Korea-Australia Rheol. J*. Vol. **16**, pp. 183-191, (2004).

[18] S. Yoon and Y. Kwon, "Finite element analysis of viscoelastic flows in a domain with geometric singularities", *Korea-Australia Rheol. J*., Vol. **17**, pp. 99-110, (2005).

[19] Y. Kwon, "Numerical analysis of viscoelastic flows in a channel obstructed by an asymmetric array of obstacles", *Korea-Australia Rheol. J.*, Vol. **18**, pp. 161-167, (2006).

[20] O.M. Coronado, D. Arora, M. Behr and M. Pasquali, "A simple method for simulating viscoelastic fluid flows with a generalized log-conformation formulation", *J. Non-Newt. Fluid Mech*. Submitted, (2006).

[21] A.M. Afonso, M.A. Alves, F.T. Pinho and P.J. Oliveira, "Application of the Log-Conformation Tensor Approach to Finite-Volume Predictions of Viscoelastic Flows", *I Conferencia Nacional de Métodos Numéricos em Mecânica dos Fluidos e Termodinâmica*, Ed. C. Pina et al., p. 36, (2006).

[22] A. Afonso, M.A. Alves, F.T. Pinho and P.J. Oliveira. "Benchmark Calculations of Viscoelastic Flows with a Finite-Volume Method Using the Log-Conformation Approach", *3rd Annual European Rheology Conference*, April 27-29, Crete, Greece, (2006).

[23] M.A. Alves, F.T. Pinho and P.J. Oliveira, "Effect of a high-resolution differencing scheme on finite-volume predictions of viscoelastic flows". *J. Non-Newt. Fluid Mech*. Vol. **93**, pp. 287-314, (2000).

[24] M.A. Alves, P.J. Oliveira and F.T. Pinho, "Benchmark solutions for the flow of Oldroyd-B and PTT fluids in planar contractions", *J. Non-Newt. Fluid Mech*. Vol. **110**, pp. 45-75, (2003).

[25] P.J. Oliveira, F.T. Pinho and G.A. Pinto, "Numerical simulation of non-linear elastic flows with a general collocated finite-volume method", *J. Non-Newt. Fluid Mech*. Vol. **79**, pp. 1–43, (1998).

[26] M.A Alves, P.J Oliveira and F.T Pinho, "A convergent and universally bounded interpolation scheme for the treatment of advection", *Int. J. Num. Meth. Fluids*, Vol. **41** pp. 47-75, (2003).

[27] F. Dupret and J.M. Marchal, "Loss of evolution in the flow of viscoelastic fluids", *J. Non-Newt. Fluid Mech*. Vol. **20**, pp. 143–171, (1986).

[28] J. Lee, S. Yoon, Y. Kwon and S.J. Kim, "Practical comparison of differential viscoelastic constitutive equations in finite element analysis of planar 4:1 contraction

flow", *Rheol. Acta*, Vol. **44**, pp. 188–197, (2004).

[29] B.P. Leonard, "A stable accurate convective modelling procedure based on quadratic upstream interpolation", *Comput. Methods Appl. Mech. Engng.* Vol. **19**, pp. 59–98, (1979).